Macromolecular Chemistry and Physics
www.mcp-journal.de

# Aligned Tubular Conjugated Microporous Polymer Films for the Aggregation-Induced Emission-Based Sensing of Explosives

*Sang Hyun Ryu, Doo Hun Lee, Yoon-Joo Ko, Sang Moon Lee, Hae Jin Kim, Kyoung Chul Ko,* and Seung Uk Son**

**This work shows the sensing performance of conjugated microporous polymer (CMP) tubes. Aligned tubular CMP films (CMP-AT) are synthesized by a template method. The Sonogashira coupling of tetra(4-ethynyl)phenylethylene with 1,4-diiodobenzene in the cylindrical pores of anodic aluminum oxide (AAO) plates and the etching of templates result in the CMP-AT films. Due to the tetraphenylethylene moieties in the materials, the CMP-AT films show aggregation-induced emission (AIE). Based on emission-quenching behavior, the sensing performance of CMP-AT films toward model explosives, nitrotoluenes, is studied. The CMP-AT films having longer CMP tubes with thinner wall thickness show better sensing performance with the Stern–Volmer constant ($K_{sv}$) values up to 92 400 $M^{-1}$ toward 2,4-dinitrotoluene. The reduced diffusion pathway of substrates by the thin wall of the CMP tubes is critical for the AIE quenching-based sensing of nitrotoluenes. These observations indicate that the functionality of CMP materials can be further enhanced by their morphological engineering. Due to the chemical stability of CMP materials, the CMP-AT-5 film can be recycled at least five times, maintaining the original sensing performance and tubular morphology.**

## 1. Introduction

Aggregation-induced emission (AIE) is an interesting and versatile phenomenon.[1] Unlike conventional luminophores showing aggregation-caused quenching, the so-called AIEgens are specific compounds showing emission triggered by the aggregation-induced restriction of intramolecular motions.[1] One of the most intensively studied AIEgens is tetraphenylethylene showing AIE by the restricted intramolecular rotation.[1,2] AIE-based materials have been applied for various purposes, including biomedical probes and sensing of harmful compounds. Recently, Tang et al. reviewed principles and applications of AIEgens.[1]

One of the attractive features of AIE is that it often enables solid state materials to be more emissive and useful than solutions. Solid state AIE materials have been applied for the sensing of pollutants or harmful compounds.[1] While the aggregation of AIEgens results in emission, it can deter diffusion of sensing targets into solid state AIE materials. The introduction of pores to solid state AIE materials can induce efficient diffusion of sensing targets into materials, thereby enhancing sensing performance.[3] With regard to this feature, the conjugated microporous polymer (CMP) materials[4] that were prepared by the Sonogashira coupling of tetraphenylethylene derivatives[5] are attractive as sensing materials. Recently, powders and films of CMP materials bearing tetraphenylethylenes were synthesized and applied for the sensing of harmful compounds.[5d,g,i,j] In addition to the unique inner microporosity of AIE-based CMP materials, the engineering of morphological structure can enhance their sensing performance through controlling diffusion pathways of sensing targets.[6]

Recently, template-free formation of tubular CMP materials has been discovered and reported by our research group and others.[7] However, physical parameters such as the length and wall thickness of CMP tubes can be more systematically controlled by a template method using anodic aluminum oxide (AAO) plates.[8] While the morphological engineering of AIE-based solid materials has been reported,[9] as

S. H. Ryu, D. H. Lee, Prof. S. U. Son
Department of Chemistry
Sungkyunkwan University
Suwon 16419, Korea
E-mail: sson@skku.edu
Dr. Y.-J. Ko
Laboratory of Nuclear Magnetic Resonance
National Center for Inter-University Research Facilities (NCIRF)
Seoul National University
Seoul 08826, Korea
Dr. S. M. Lee, Dr. H. J. Kim
Korea Basic Science Institute
Daejeon 34133, Korea
Prof. K. C. Ko
Department of Chemistry Education
Chonnam National University
Gwangju 61186, Korea
E-mail: kcko1982@jnu.ac.kr
The ORCID identification number(s) for the author(s) of this article can be found under https://doi.org/10.1002/macp.201900157.

**DOI: 10.1002/macp.201900157**

 

far as we are aware, the aligned tubular engineering of AIE-based CMP materials was not reported.

In this work, we report the engineering of aligned tubular CMP films showing AIE (CMP-AT) and their sensing performance toward model explosives.

## 2. Experimental Section

### 2.1. General Information

SEM and TEM studies were conducted using JSM6700F and JEOL 2100F machines, respectively. The surface areas and pore size distribution diagrams were obtained through the analysis of $N_2$ sorption isotherm curves measured at 77 K using a Micromeritics ASAP2020. The pore size distribution was analyzed by the density functional theory (DFT) method. IR absorption spectra were obtained using a Bruker VERTEX 70 FT-IR spectrometer. Solid state $^{13}C$ nuclear magnetic resonance (NMR) spectra were obtained at CP/TOSS mode using a 500 MHz Bruker ADVANCE II NMR machine at the NCIRF of Seoul National University. Powder X-ray diffraction (PXRD) patterns were obtained using a Rigaku MAX-2200 machine. Diffuse reflectance spectra were obtained using a SHIMADZU UN-3600. The absorption spectra of CMP-AT films were obtained from the reflectance spectra. Emission spectra were obtained in ethanol with an excitation wavelength of 410 nm using a JASCO FP-6200 spectrometer. Thermogravimetric analysis (TGA) curves were obtained under $N_2$ using a Seiko Exstar 7300.

### 2.2. Synthesis of CMP-AT Films

AAO plates with a hole diameter of 300 nm and hole depths of 1, 2, and 5 μm were purchased from Inredox company (refer to Figure S1, Supporting Information). Tetra(4-ethynylphenyl)ethylene was prepared by the synthetic procedures reported in the literature.[10] For the preparation of CMP-AT-5, an AAO plate with a hole diameter of 300 nm and a hole depth of 5 μm was cut to a plate of 6.5 cm × 2.5 cm, washed with acetone, and dried under vacuum oven at 80 °C for 8 h. AAO plate, triethylamine (35 mL), and toluene (25 mL) were added to a flame-dried 100 mL flask with a Rodaviss joint. $(PPh_3)_2PdCl_2$ (2.6 mg, 3.7 μmol) and CuI (0.70 mg, 3.7 mmol) were dispersed in toluene (5 mL) by sonication and added to the reaction mixture, which was then stirred at room temperature for 1.5 h. Tetra(4-ethynylphenyl) ethylene (26 mg, 0.060 mmol) and 1,4-diiodobenzene (39 mg, 0.12 mmol) were dissolved in tetrahydrofuran (5 mL) by sonication and added to the reaction mixture, which was then stirred at room temperature for 20 min and then, heated at 90 °C for 24 h without stirring. After being cooled to room temperature, the CMP@AAO plate was taken out, washed with ethanol, sonicated for 2 min in ethanol to remove CMP powders adsorbed on surface, and dried at room temperature. To obtain the CMP-AT-5 film, the CMP@AAO plate was spin-coated using poly(methyl methacrylate) (950 PMMA C4, MicroChem; 1 mL) and dried at room temperature under air. The used spin coater was a SP-7200GT spin coater (Intec System). The spin coating conditions were 10 s at 1000 rpm and 10 s at 2000 rpm. The CMP@AAO/PMMA plate was cut to a small plate of 0.5 cm × 0.5 cm, added to 3M $H_3PO_4$ solution (30 mL), and heated at 80 °C for 12 h. The resultant CMP-AT-5/PMMA film was added to acetone (200 mL) to remove PMMA, which was repeated thrice. The resultant CMP-AT-5 film in an ethanol solution was transferred to poly(ethylene terephthalate) film and dried at room temperature under air.

For the preparation of CMP-AT-1 and CMP-AT-2, the same procedures of CMP-AT-5 were applied except that AAO plates with pore depths of 1 and 2 μm, respectively, were used instead of AAO plate with a pore depth of 5 μm. For the preparation of CMP-AT-5T film, the same procedures of CMP-AT-5 were applied except that tetra(4-ethynylphenyl) ethylene (51 mg, 0.12 mmol) and 1,4-diiodobenzene (79 mg, 0.24 mmol) were used. For the preparation of CMP-AT-5S film, the same procedures of CMP-AT-5 were applied except that tetra(4-ethynylphenyl)ethylene (6.4 mg, 0.015 mmol) and 1,4-diiodobenzene (9.9 mg, 0.030 mmol) were used. Bulk CMP-A materials were prepared by the synthetic method reported in the literature.[5j]

### 2.3. Procedures of Sensing Tests

A slide glass plate was cut to a small plate of 1.3 cm × 7.5 cm. A carbon tape (0.5 cm × 2 cm) was attached to the slide glass plate. CMP-AT film (0.5 cm × 0.5 cm) was attached on the carbon tape. The CMP-AT film was dipped into pure ethanol solution (3 mL) for 1 h for the complete diffusion of the solvent into the materials, resulting in no changes of emission intensity. The emission intensity ($I_o$) was measured using an excitation wavelength of 410 nm. Analyte (2,4-dinitrotoluene [DNT], 2-nitrotoluene [2NT], 4-nitrotoluene [4NT], 4-chlorotoluene [4CT], and toluene [Tol]) ethanol solutions with 0.00250, 0.00500, 0.0100, 0.0200, 0.0500, 0.125, and 0.500 mM concentration were prepared by diluting stock solution. The CMP-AT film retrieved from measurement of $I_o$ was dipped into the analyte solution (3 mL). After 1 h, the emission intensity ($I$) was measured using an excitation wavelength of 410 nm. The Stern–Volmer constants ($K_{sv}$) were obtained by the Stern–Volmer plot ($I_o/I$ versus [$M$], [$M$]: concentration of analyte solution) based on the following equation, $I_o/I = K_{sv}[M] + 1$. All measurements were repeated thrice and the results treated statistically were shown in text. For recycle tests, 0.500 mM DNT solution was used for CMP-AT-5 film. After emission quenching, the retrieved CMP-AT-5 film was washed with ethanol and used for the next run.

### 2.4. Procedures of DFT Simulation

In order to understand the fluorescent sensing mechanism of CMP-AT-5 film, DFT calculations were performed.[5j] Representative three model systems, that is, CMP-AT-5-1, CMP-AT-5-5, and CMP-AT-5-poly were designed to investigate the trend of frontier orbital energy levels from a monomeric case

to an infinite polymeric case. For three model systems as well as six target compounds (2,4,6-trinitrotoluene [TNT], DNT, 2NT, 4NT, 4CT, and Tol), geometrical optimizations and the HOMO and LUMO energy level calculations were simulated at B3LYP/light-tier-1 level of theory using FHI-aims code.[11] The convergence criterion was set to $10^{-2}$ eV Å$^{-1}$ for geometrical relaxation.

It should be noted that for CMP-AT-5-poly case, PBE/light-tier-1 setting was adopted for the optimization of both nucleus geometries and unit cell parameters owing to enormous computational costs for periodic boundary condition calculation with hybrid B3LYP functional. Also, the convergence criterion setting was reduced to $2 \times 10^{-2}$ eV Å$^{-1}$. Then, a single-point calculation with B3LYP functional was carried out to predict the HOMO and LUMO energy levels of CMP-AT-5-poly. The optimized unit cell parameters (*a*, *b*, and *c*) of CMP-AT-5-poly were computed as 33.49 Å × 22.97 Å × 39.34 Å involving a vacuum space 30 Å along *c*-axis.

## 3. Result and Discussion

**Figure 1** shows a synthetic scheme for the CMP-AT films. Using tetra(4-ethynylphenyl)ethylene (0.060 mmol)[10] and 2 eq. 1,4-diiodobenzene as building blocks, CMP materials were formed in the cylindrical pores of AAO plates through the Sonogashira coupling. Acid etching of the AAO plates resulted in the CMP-AT films. The length of the CMP tubes in the CMP-AT films was controlled by changing the pore depths of AAO plates from 1 µm to 2 and 5 µm (Figures S1 and S2, Supporting Information). The corresponding films were denoted as CMP-AT-1, CMP-AT-2, and CMP-AT-5, respectively. The

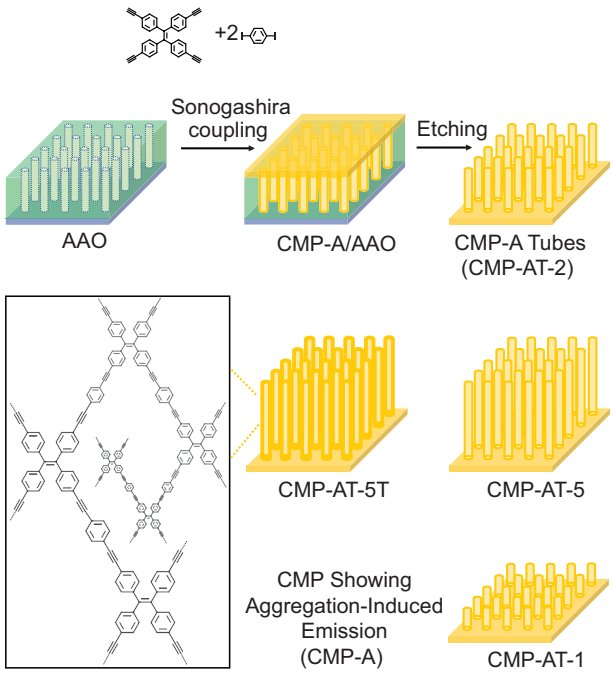


**Figure 1.** A synthetic scheme of CMP-AT films.

diameter (300 nm) of the CMP tubes in the CMP-AT films replicated the pore diameter of the original AAO templates (Figures S1 and S2, Supporting Information). The wall thickness of the CMP tubes in the CMP-AT-5 films was controlled by changing the amount of tetra(4-ethynylphenyl)ethylene from 0.060 mmol to 0.12 and 0.015 mmol. The materials prepared using 0.12 mmol of tetra(4-ethynylphenyl)ethylene was denoted as CMP-AT-5T. When we reduced the amount of the tetra(4-ethynylphenyl)ethylene building block to 0.015 mmol, the CMP tubes in the film (denoted as CMP-AT-5S) could not stand due to the thin wall thickness of 20–25 nm (Figure S3, Supporting Information).

Overall morphology and wall thickness of the CMP tubes in the CMP-AT films were investigated by scanning (SEM) and transmission electron microscopy (TEM) (**Figure 2** and Figures S2 and S3, Supporting Information). As shown in the SEM images in Figures 2a and S2, Supporting Information, CMP tubes with a length of 1 µm in CMP-AT-1 were relatively rigid, compared with those in CMP-AT-5 (vide infra), and well aligned. TEM image of CMP-AT-1 confirmed the tubular morphology, showing empty inner structure and a wall thickness of 45–50 nm (Figure 2b).

Similar to CMP-AT-1, the CMP tubes in CMP-AT-2 were relatively rigid and well aligned with the increased length of 2 µm (Figure 2c and Figure S2, Supporting Information). The TEM image of CMP-AT-2 confirmed the tubular morphology of CMP tubes, showing an empty inner structure and a wall thickness of 45–50 nm (Figure 2d). When the length of the CMP tubes increased to 5 µm, the CMP tubes in CMP-AT-5 were quite flexible. In contrast, those in CMP-AT-5T were relatively rigid (Figure 2e,g and Figure S2, Supporting Information). The TEM images of CMP-AT-5 and CMP-AT-5T confirmed the tubular morphology (Figure 2f,h). The wall thickness of the CMP tubes increased from ≈45 nm (CMP-AT-5) to 55–60 nm (CMP-AT-5T) (Figure 2f,h). The SEM images of all CMP-AT films showed good homogeneity of aligned tubular morphologies (Figure 2a,c,e,g).

The surface areas and microporosity of CMP-AT films were characterized by the analysis of $N_2$ sorption isotherm curves obtained at 77 K. The surface areas of CMP-AT-1, CMP-AT-2, CMP-AT-5, and CMP-AT-5T were measured to be 182, 242, 505, and 660 m$^2$ g$^{-1}$, respectively, (**Figure 3**a). The pore size distribution analysis based on the DFT method confirmed the microporosity (pore sizes <2 nm) of all CMP-AT films (Figure 3b). Unfortunately, we could not characterize the porosity of CMP-AT-5S due to the poor quality of materials (Figure S3, Supporting Information). According to the PXRD studies, CMP-AT films were all noncrystalline, matching well with the conventional properties of CMP materials in the literature[12] (Figure S4, Supporting Information). Infrared (IR) absorption spectra of all CMP-AT films were the same, indicating that their chemical structures are nearly the same (Figure 3c). Two major vibration peaks were observed at 1511 and 834 cm$^{-1}$, which correspond to the C=C and C−H vibrations, respectively, of aromatic groups in CMP-AT materials.[5j] Solid state $^{13}$C NMR spectra of all CMP-AT films showed $^{13}$C peaks at 90 and 110–145 ppm (Figure 3d), corresponding to the internal alkynes and sp$^2$ carbons in the CMP materials,[5j] indicating that the CMP materials in this

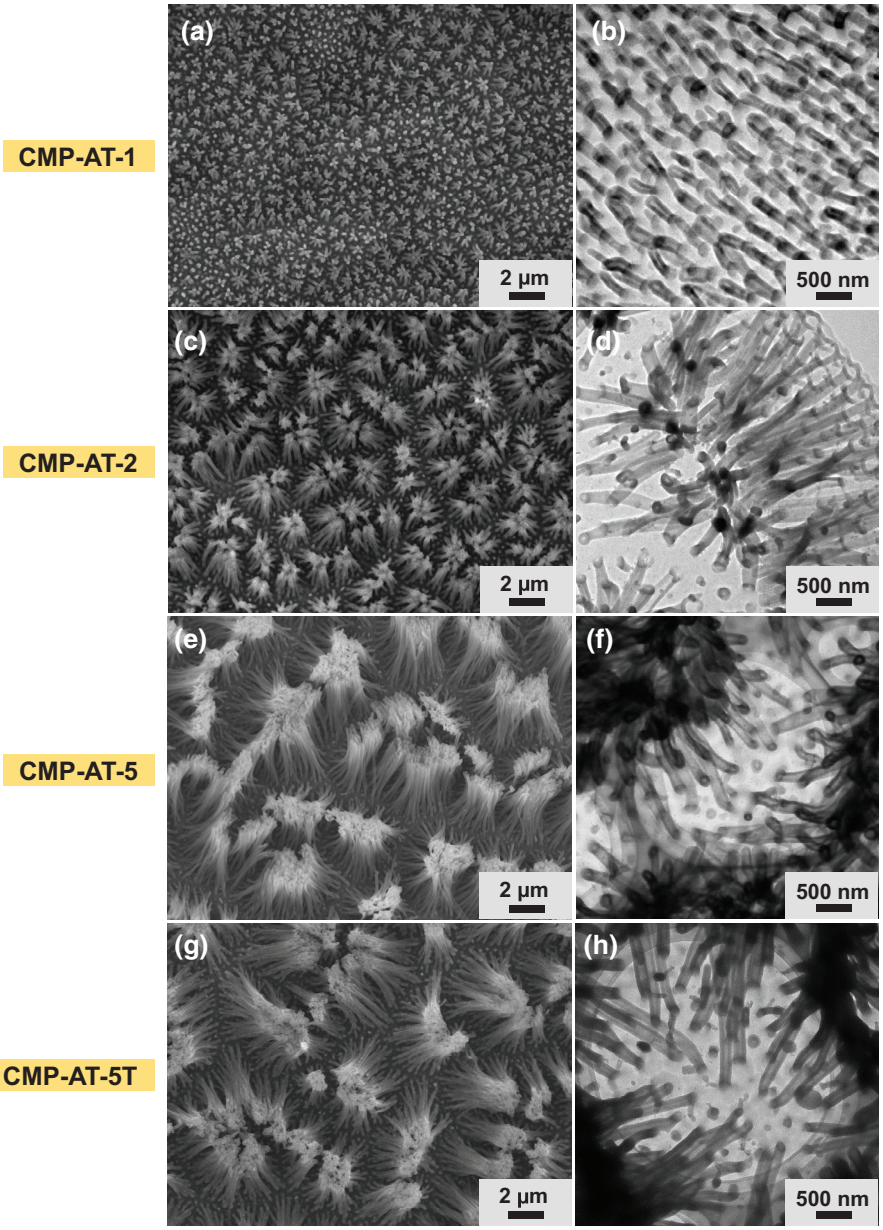


**Figure 2.** SEM and TEM images of a,b) CMP-AT-1; c,d)CMP-AT-2; e,f) CMP-AT-5; and g,h) CMP-AT-5T films.

work were formed by the Sonogashira coupling of the used building blocks.

The optical properties of CMP-AT films were investigated by diffuse reflectance and emission spectroscopy (Figure 3e). While major absorption bands shifted gradually from 355 nm (CMP-AT-1) to 360 (CMP-AT-2), 365, (CMP-AT-5) and 375 nm (CMP-AT-5T), due to the elongated conjugated length, the emission bands did not shift significantly and appeared at 520–523 nm (Figure 3e). Compared with non-emissive property of tetra(4-ethynylphenyl)ethylene in reaction solution, the CMP-AT films were all emissive, indicating their AIE behaviors. The fluorescence quantum yield of CMP-AT-5 was measured to be 30.0% using $[Ru(bpy)_3](PF_6)_2$ as a comparative compound.[13] According to TGA, the CMP-AT films were stable up to 265 °C (Figure 3f).

Considering the emission properties of CMP-AT films, we studied their emission quenching–based sensing performance toward model explosives, nitrotoluenes.[14] Unfortunately, due to safety regulations, we could not synthesize and obtain TNT. In addition, recently, 2,4,6-trinitrophenol became commercially unavailable. Therefore, we tested DNT, 2NT, and 4NT as target-sensing compounds, compared with 4CT and Tol (**Figure 4**a).

As shown in Figure 4b,c, CMP-AT-5 exhibited better sensing performance toward DNT, compared with those toward 2NT and 4NT. Through the Stern–Volmer plot, $K_{sv}$ values were measured to be 92 400, 59 600, and 40 900 $M^{-1}$ for DNT, 2NT, and 4NT, respectively (Figure 4d and **Table 1**). Interestingly, 4CT and Tol did not show convincing emission quenching of CMP-AT-5 film (Figure 4c).

In order to understand the observed sensing selectivities of CMP-AT-5, we simulated the LUMO and HOMO energy levels of CMP-AT materials based on the DFT[5j,11] (**Figure 5** and Figure S5, Supporting Information). Although the inner network structure of CMP-AT materials would not be regular but amorphous, we systematically extended conjugation domains eventually to limitless (Figure 5a).

Based on the optimized geometrical structures of model CMP-AT systems, LUMO and HOMO energy levels were simulated to be −2.31 to −2.97 eV and −5.52 to −5.44 eV, respectively. In comparison, LUMO energy levels of TNT, DNT, 2NT, and 4NT were simulated to be −3.96, −3.44, −2.77, and −2.82 eV, respectively (Figure 5b). Thus, it can be expected that the emission quenching of CMP-AT-5 by nitrotoluenes is reasonable due to possible electron transfer from the excited state of CMP-AT to the LUMO energy levels of nitrotoluenes. In comparison, LUMO energy levels of 4CT and Tol were simulated to be −0.78 and −0.39 eV, respectively, indicating that electron transfer from excited state of CMP-AT to the LUMO of these substrates is not reasonable.

Next, we studied the effects of length and wall thickness of CMP tubes on the sensing performance of CMP-AT films (**Figure 6**a–e). In addition, we prepared bulk CMP-A as a control material through the Sonogashira coupling of tetra(4-ethynylphenyl)ethylene with 1,4-diiodobezne without using AAO templates[5j] (Figure S6, Supporting Information). When we

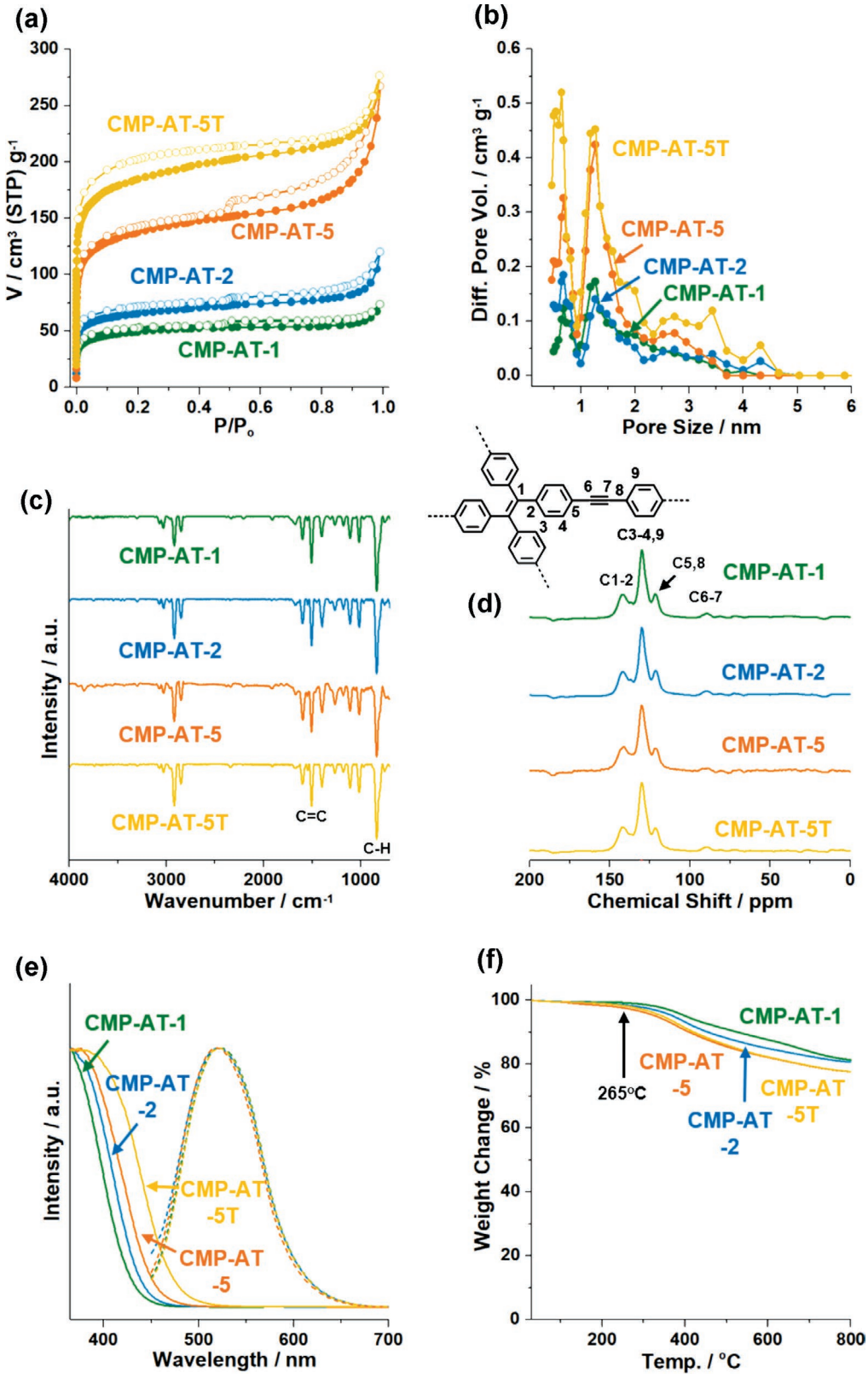


**Figure 3.** a,b) $N_2$ adsorption–desorption isotherm curves obtained at 77 K and pore size distribution diagrams based on the density functional theory (DFT) method; c) IR absorption spectra; d) solid state $^{13}C$ NMR; e) UV–vis absorption (solid lines) and emission (dotted lines, excitation wavelength: 410 nm) spectra; and f) TGA curves of CMP-AT-1, CMP-AT-2, CMP-AT-5, and CMP-AT-5T.

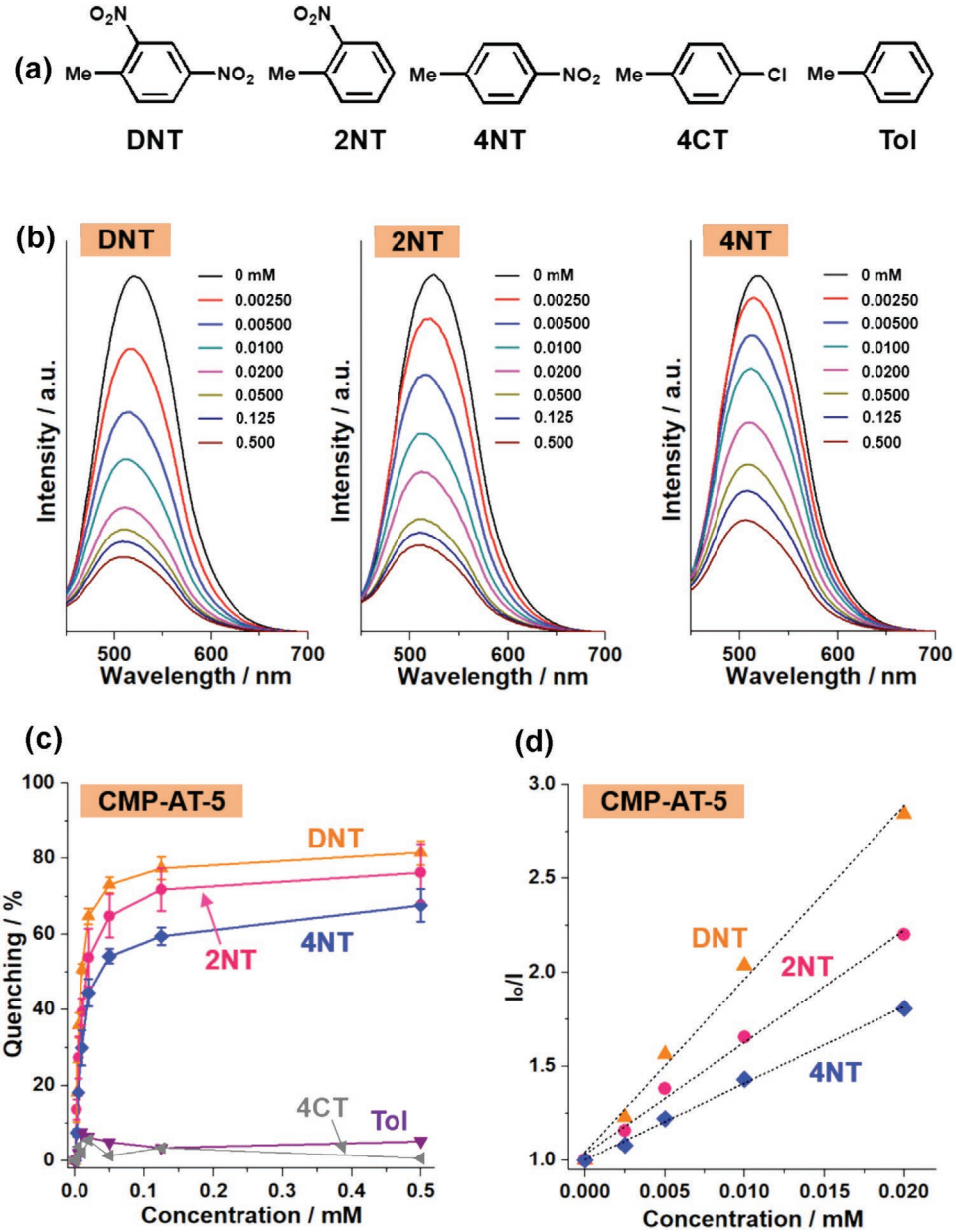


**Figure 4.** a) Sensing target compounds used in this study. b) Emission spectra of CMP-AT-5 depending on the concentration of DNT, 2NT, and 4NT. c) Emission-quenching behaviors of CMP-AT-5 by nitrotoluenes and 4-chlorotoluene and toluene (average values of three measurements, solvent: ethanol, $\lambda_{ex}$: 410 nm). d) The Stern–Volmer plot of emission quenching of CMP-AT-5 by nitrotoluenes.

compared CMP-AT-1, CMP-AT-2, and CMP-AT-5, the order of sensing performance toward DNT was CMP-AT-5 > CMP-AT-2 > CMP-AT-1 (Figure 6a,d,e). The $K_{sv}$ values of CMP-AT-5, CMP-AT-2, and CMP-AT-1 were measured to be 92 400, 75 700, and 61 200 $M^{-1}$, respectively (Figure 6e and Table 1). The observed order of sensing performance in CMP-AT-1, CMP-AT-2, and CMP-AT-5 can be attributed to the increasing order of surface areas. In addition, the CMP-AT-5 showed much better sensing performance toward DNT than the CMP-AT-5T and bulk CMP-A. The $K_{sv}$ values of CMP-AT-5T, CMP-AT-5S, and bulk CMP-A were measured to be 48 500, 150 000, and 12 800 $M^{-1}$, respectively (Figure 6a–e and Figure S3, Supporting Information; Table 1)

The observed trend indicates that the wall thickness of the CMP tubes in the CMP-AT is a critical factor in the AIE-based sensing of nitrotoluenes. As the walls of CMP tubes became thinner, the sensing performance was significantly enhanced. It indicates that although CMP materials have inner microporosity, the further control of the diffusion pathways of substrates through morphological engineering is important to enhance the sensing performance. The detection limit (LOD) of CMP-AT-5 toward DNT was calculated to be 0.37 ppm. Moreover,

**Table 1.** $K_{sv}$ values of CMP-AT films for the emission quenching by nitrotoluenes (average results of three sets).

| Entry | Materials | Surface area[a)] [$m^2$ $g^{-1}$] | Wall thickness [nm] | Substrate | $K_{SV}$[b)] [$M^{-1}$] |
|---|---|---|---|---|---|
| 1 | CMP-AT-1 | 182 | 45–50 | DNT | 61 200 |
| 2 | CMP-AT-2 | 242 | 45–50 | DNT | 75 700 |
| 3 | CMP-AT-5 | 505 | ≈45 | DNT | 92 400 |
| 4 | CMP-AT-5 | 505 | ≈45 | 2NT | 59 600 |
| 5 | CMP-AT-5 | 505 | ≈45 | 4NT | 40 900 |
| 6 | CMP-AT-5T | 660 | 55–65 | DNT | 48 500 |
| 7 | CMP-AT-5S | —[c)] | 20–25 | DNT | 150 000 |
| 8 | Bulk CMP-A | 242 | 300–1000 | DNT | 12 800 |

Conditions: ethanol, $\lambda_{ex}$: 410 nm; [a)]Surface areas based on the BET theory; [b)]$R^2$ of a linear regression = 0.99 for the Stern–Volmer plot; [c)]The surface area could not be measured due to the poor quality of materials (also, refer to Figure S3, Supporting Information).

the $K_{sv}$ value (92 400 $M^{-1}$) of CMP-AT-5 toward DNT is superior to those of recent emissive CMP materials in the literature,[15] which resulted from not only the thin wall thickness but also the aligned tubular morphology facilitating the contact of sensing targets with the CMP tubes (Table S1, Supporting Information)

Another merit of CMP materials is their chemical stability. Considering stability shown in Figure 3f, we performed

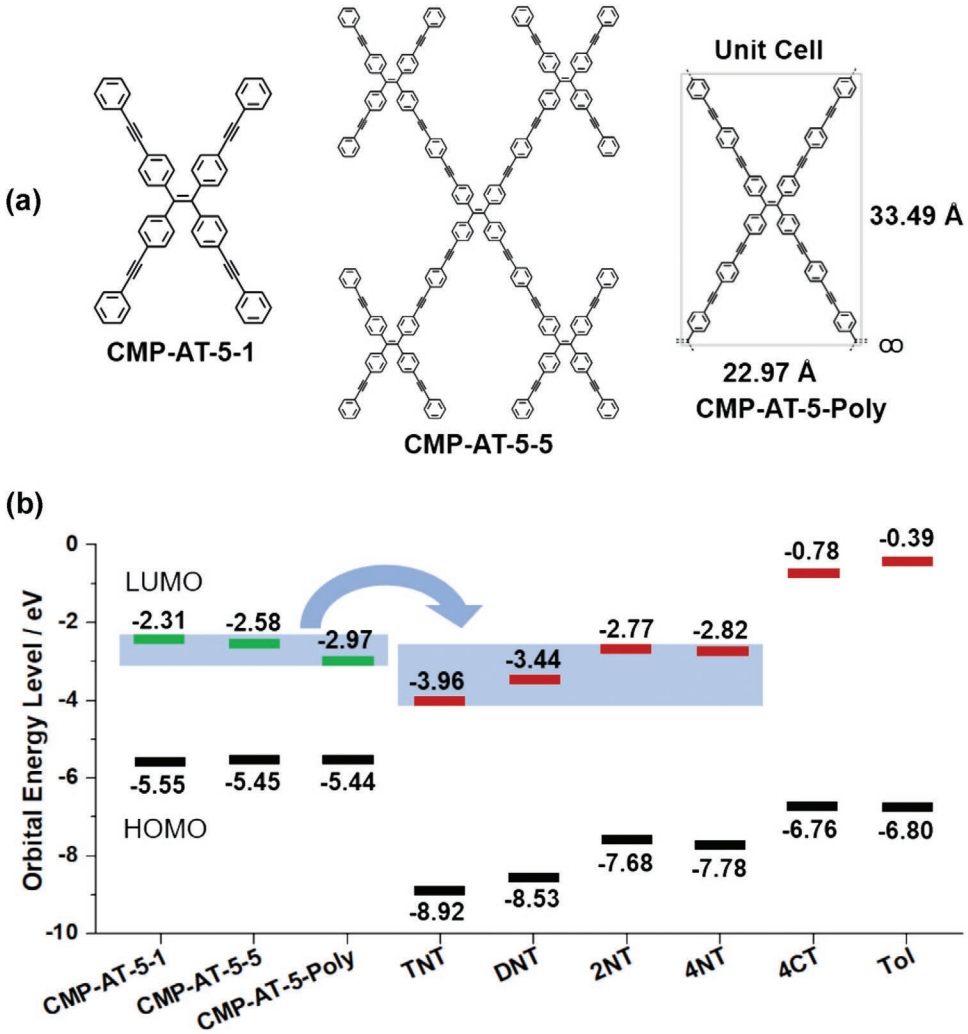


**Figure 5.** a) Model systems for computational simulation of CMP-AT-5. b) Simulated LUMO-HOMO energy levels of model systems of CMP-AT-5, nitrotoluenes, 4-chlorotoluene, and toluene.

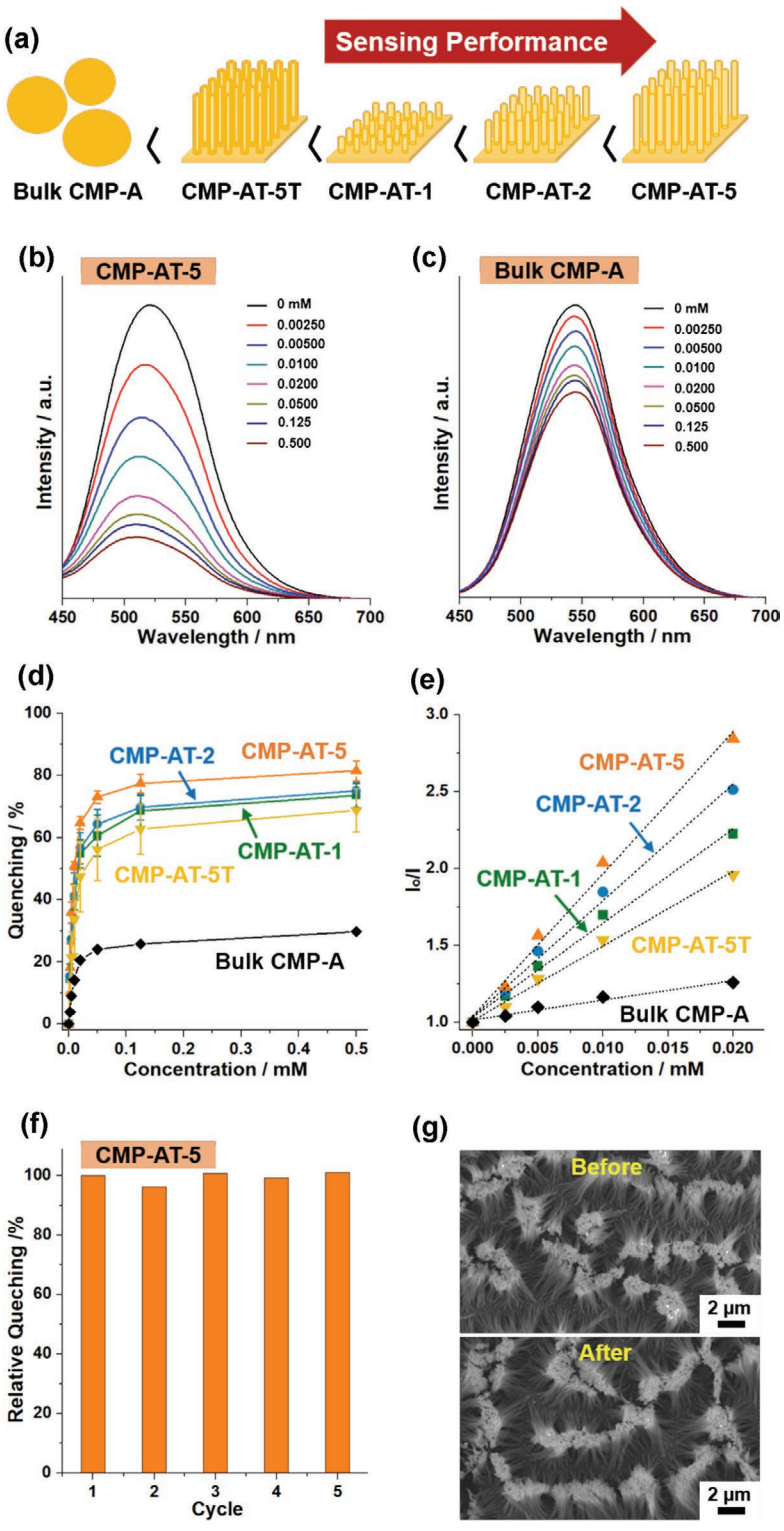


**Figure 6.** a) Morphological structure–dependent sensing performance of bulk CMP-A and CMP-AT materials. Emission spectra of b) CMP-AT-5 and c) bulk CMP-A materials depending on the concentration of DNT (solvent: ethanol, $\lambda_{ex}$: 410 nm). d) Emission-quenching behavior of CMP-AT-1, CMP-AT-2, CMP-AT-5, and CMP-AT-5T by DNT (solvent: ethanol, $\lambda_{ex}$: 410 nm) and e) corresponding Stern–Volmer plots. f) Recycle tests (solvent: ethanol, $\lambda_{ex}$: 410 nm) of CMP-AT-5 in the sensing of DNT (0.500 mM). The quenching degree (90%) of the first run was defined as relative quenching of 100% for comparison. g) SEM images of CMP-AT-5 before and after five successive sensing tests.

recycle tests of CMP-AT-5. As shown in Figure 6f, the CMP-AT-5 could be recycled for the sensing of DNT at least five times through simple washing, maintaining 96, 101, 99, and 101% of the quenching degree of the first run at second, third, fourth, and fifth runs, respectively. According to the SEM and IR absorption analysis, the CMP-AT-5 that was recovered after five successive sensing tests showed the complete retention of the original tubular morphologies and chemical structure (Figure 6g and Figure S7, Supporting Information).

## 4. Summary and Conclusions

In conclusion, CMP-AT films with aligned CMP tubes were engineered using AAO templates and applied for the sensing of nitrotoluenes based on the quenching of AIE. The sensing performance of CMP-AT films was dependent on the length and wall thickness of CMP tubes. Especially, the CMP tubes with thinner wall thickness showed much enhanced sensing performance toward nitrotoluenes. Among the CMP-AT films in this study, the CMP-AT-5 with a tube length of 5 μm and a wall thickness of ≈45 nm showed a $K_{sv}$ value up to 92 400 $M^{-1}$ for DNT. This study implies that in addition to inner microporosity, the reduced diffusion pathway by the thin wall thickness of CMP tubes can enhance the AIE quenching–based sensing performance. We believe that more various functional CMP tube films can be engineered by the synthetic method presented in this work through the scanning of the tailored building blocks.

## Supporting Information

Supporting Information is available from the Wiley Online Library or from the author.

## Acknowledgements

This work was supported by the Basic Science Research Program (2016R1E1A1A01941074) through the National Research Foundation of Korea (NRF) funded by the Ministry of Science, ICT, and Future Planning. K.C.K acknowledges the financial support by the Basic Science Research Program (2016R1A6A3A11933303) through the NRF of Korea funded by the Ministry of Education.

## Conflict of Interest

The authors declare no conflict of interest.

## Keywords

aggregation-induced emission, microporous organic polymers, sensing, tubes

Received: April 14, 2019
Published online: May 10, 2019

[1] J. Mei, N. L. C. Leung, R. T. K. Kwok, J. W. Y. Lam, B. Z. Tang, *Chem. Rev.* **2015**, *115*, 11718.

[2] J. Mei, Y. Hong, J. W. Y. Lam, A. Qin, Y. Tang, B. Z. Tang, *Adv. Mater.* **2014**, *26*, 5429.

[3] a) X.-M. Hu, Q. Chen, D. Zhou, J. Cao, Y.-J. He, B.-H. Han, *Polym. Chem.* **2011**, *2*, 1124; b) N. B. Shustova, B. D. McCarthy, M. Dincă, *J. Am. Chem. Soc.* **2011**, *133*, 20126; c) R. Hu, J. W. Y. Lam, J. Liu, H. H. Y. Sung, I. D. Williams, Z. Yue, K. S. Wong, M. M. F. Yuen, B. Z. Tang, *Polym. Chem.* **2012**, *3*, 1481; d) M. Zhang, G. Feng, Z. Song, Y.-P. Zhou, H.-Y. Chao, D. Yuan, T. T. Y. Tan, Z. Guo, Z. Hu, B. Z. Tang, B. Liu, D. Zhao, *J. Am. Chem. Soc.* **2014**, *136*, 7241; e) Z. Wei, Z.-Y. Gu, R. K. Arvapally, Y.-P. Chen, R. N. McDougald, Jr., J. F. Ivy, A. A. Yakovenko, D. Feng, M. A. Omary, H.-C. Zhou, *J. Am. Chem. Soc.* **2014**, *136*, 8269.

[4] a) L. Tan, B. Tan, *Chem. Soc. Rev.* **2017**, *46*, 3322; b) N. Chaoui, M. Trunk, R. Dawson, J. Schmidt, A. Thomas, *Chem. Soc. Rev.* **2017**, *46*, 3302; c) S. Das, P. Heasman, T. Ben, S. Qiu, *Chem. Rev.* **2017**, *117*, 1515; d) R. Dawson, A. I. Cooper, D. J. Adams, *Prog. Polym. Sci.* **2012**, *37*, 530; e) Y. Xu, S. Jin, H. Xu, A. Nagai, D. Jiang, *Chem. Soc. Rev.* **2013**, *42*, 8012; f) F. Vilela, K. Zhang, M. Antonietti, *Energy Environ. Sci.* **2012**, *5*, 7819; g) N. B. McKeown, P. M. Budd, *Chem. Soc. Rev.* **2006**, *35*, 675.

[5] a) Q. Chen, J.-X. Wang, F. Yang, D. Zhou, N. Bian, X.-J. Zhang, C.-G. Yan, B.-H. Han, *J. Mater. Chem.* **2011**, *21*, 13554; b) Y. Xu, L. Chen, Z. Guo. A. Nagai, D. Jiang, *J. Am. Chem. Soc.* **2011**, *133*, 17622; c) V. M. Suresh, S. Bonakala, S. Roy, S. Balasubramanian, T. K. Maji, *J. Phys. Chem. C* **2014**, *118*, 24369; d) C. Gu, N. Huang, Y. Wu, H. Xu, D. Jiang, *Angew. Chem., Int. Ed.* **2015**, *54*, 11540; e) K. Yuan, P. Guo-Wang, T. Hu, L. Shi, R. Zeng, M. Forster, T. Pichler, Y. Chen, U. Scherf, *Chem. Mater.* **2015**, *27*, 7403; f) H. Li, X. Ding, B.-H. Han, *RSC Adv.*. **2016**, *6*, 51411; g) Y. Cui, Y. Liu, J. Liu, J. Du, Y. Yu, S. Wang, Z. Liang, J. Yu, *Polym. Chem.* **2017**, *8*, 4842; h) H. Liu, H. Liu, *J. Mater. Chem. A* **2017**, *5*, 9156; i) A. Palma-Cando, D. Woitassek, G. Brunklaus, U. Scherf, *Mater. Chem. Front.* **2017**, *1*, 1118; j) D. H. Lee, K. C. Ko, J. H. Ko, S. Y. Kang, S. M. Lee, H. J. Kim, Y.-J. Ko, J. Y. Lee, S. U. Son, *ACS Macro Lett.* **2018**, *7*, 651.

[6] a) N. Kang, J. H. Park, M. Jin, N. Park, S. M. Lee, H. J. Kim, J. M. Kim, S. U. Son, *J. Am. Chem. Soc.* **2013**, *135*, 19115; b) J. H. Park, J. H. Ko, S. J. Hong, Y. J. Shin, N. Park, S. Kang, S. M. Lee, H. J. Kim, S. U. Son, *Chem. Mater.* **2015**, *27*, 5845; c) C. W. Kang, J. Choi, J. H. Ko, S.-K. Kim, Y.-J. Ko, S. M. Lee, H. J. Kim, J. P. Kim, S. U. Son, *J. Mater. Chem. A* **2017**, *5*, 5696; d) K. Cho, J. Yoo, H.-W. Noh, S. M. Lee, H. J. Kim, Y.-J. Ko, H.-Y. Jang, S. U. Son, *J. Mater. Chem. A* **2017**, *5*, 8922.

[7] a) J. Chun, J. H. Park, J. Kim, S. M. Lee, H. J. Kim, S. U. Son, *Chem. Mater.* **2012**, *24*, 3458; b) Z. Xiang, H. Sun, Z. Zhu, W. Liang, B. Yang, A. Li, *RSC Adv.* **2015**, *5*, 24893; c) L. Bao, H. Sun, Z. Zhu, W. Liang, P. Mu, J. Zang, A. Li, *Mater. Lett.* **2016**, *178*, 5; d) J. G. Kim, M. C. Cha, J. Lee, T. Choi, J. Y. Chang, *ACS Appl. Mater. Interfaces* **2017**, *9*, 38081.

[8] a) R. O. Al-Kaysi, T. H. Ghaddar, G. Guirado, *J. Nanomater.* **2009**, *2009*, 7; b) S. H. Ryu, C. W. Kang, J. Choi, Y. Myung, Y.-J. Ko, S. M. Lee, H. J. Kim, S. U. Son, *ACS Appl. Mater. Interfaces* **2018**, *10*, 6815.

[9] a) L. Heng, J. Zhai, A. Qin, Y. Zhang, Y. Dong, B. Z. Tang, L. Jiang, *ChemPhysChem* **2007**, *8*, 1513; b) K. H. Cheng, Y. Zhong, B. Y. Xie, Y. Q. Dong, Y. Hong, J. Z. Sun, B. Z. Tang, K. S. Wong, *J. Phys. Chem. C* **2008**, *112*, 17507.

[10] Y. Xu, D. Chang, S. Feng, C. Zhang, J.-X. Jiang, *New J. Chem.* **2016**, *40*, 9415.

[11] V. Blum, R. Gehrke, F. Hanke, P. Havu, V. Havu, X. Ren, K. Reuter, M. Scheffler, *Comput. Phys. Commun.* **2009**, *180*, 2175.

[12] a) J.-X. Jiang, F. Su, A. Trewin, C. D. Wood, H. Niu, J. T. A. Jones, Y. Z. Khimyak, A. I. Cooper, *J. Am. Chem. Soc.* **2008**, *130*, 7710; b) J.-X. Jiang, F. Su, A. Trewin, C. D. Wood, N. L. Campbell, H. Niu, C. Dickinson, A. Y. Ganin, M. J. Rosseinsky, Y. Z. Khimyak, A. I. Cooper, *Angew. Chem., Int. Ed.* **2007**, *46*, 8574.

[13] K. Suzuki, A. Kobayashi, S. Kaneko, K. Takehira, T. Yoshihara, H. Ishida, Y. Shiina, S. Oishi, S. Tobita, *Phys. Chem. Chem. Phys.* **2009**, *11*, 9850.

[14] a) X. Sun, Y. Wang, Y. Lei, *Chem. Soc. Rev.* **2015**, *44*, 8019; b) Y.-W. Wu, A.-J. Qin, B. Z. Tang, *Chin. J. Polym. Sci.* **2017**, *35*, 141.

[15] a) Z. Xiang, D. Cao, *Macromol. Rapid Commun.* **2012**, *33*, 1184; b) X. Liu, Y. Xu, D. Jiang, *J. Am. Chem. Soc.* **2012**, *134*, 8738; c) L. Sun, Z. Liang, J. Yu, R. Xu, *Polym. Chem.* **2013**, *4*, 1932; d) X. Wu, H. Li, B. Xu, H. Tong, L. Wang, *Polym. Chem.* **2014**, *5*, 4521; e) Y. Zhang, S. A, Y. Zou, X. Luo, Z. Li, H. Xia, X. Liu, Y. Mu, *J. Mater. Chem. A* **2014**, *2*, 13422; f) W. Wei, R. Lu, S. Tang, X. Liu, *J. Mater. Chem. A* **2015**, *3*, 4604; g) J. H. Ko, J. H. Moon, N. Kang, J. H. Park, H.-W. Shin, N. Park, S. Kang, S. M. Lee, H. J. Kim, T. K. Ahn, J. J. Lee, S. U. Son, *Chem. Commun.* **2015**, *51*, 8781; h) N. Sang, C. Zhan, D. Cao, *J. Mater. Chem. A* **2015**, *3*, 92; i) N. Park, K. C. Ko, H. W. Shin, S. M. Lee, H. J. Kim, J. Y. Lee, S. U. Son, *J. Mater. Chem. A* **2016**, *4*, 8010; j) T.-M. Geng, S.-N. Ye, Y. Wang, H. Zhu, X. Wang, X. Liu, *Talanta* **2017**, *165*, 282; k) T. Geng, Z. Zhu, X. Wang, H. Xia, Y. Wang, D. Li, *Sens. Actuators, B* **2017**, *244*, 334.

 